Faraday-Shielded dc Stark-Shift-Free Optical Lattice Clock

K. Beloy, X. Zhang, W. F. McGrew, N. Hinkley, T. H. Yoon, D. Nicolodi, R. J. Fasano, S. A. Schäffer, R. C. Brown, and A. D. Ludlow

Faraday-shielded, DC Stark-free optical lattice clock

K. Beloy,[1, *] X. Zhang,[1, †] W. F. McGrew,[1, 2] N. Hinkley,[1, 2, ‡] T. H. Yoon,[1, §] D. Nicolodi,[1] R. J. Fasano,[1, 2] S. A. Schäffer,[1, ¶] R. C. Brown,[1, **] and A. D. Ludlow[1]

[1]*National Institute of Standards and Technology, 325 Broadway, Boulder, Colorado 80305, USA*
[2]*Department of Physics, University of Colorado, Boulder, Colorado 80309, USA*

We demonstrate the absence of a DC Stark shift in an ytterbium optical lattice clock. Stray electric fields are suppressed through the introduction of an in-vacuum Faraday shield. Still, the effectiveness of the shielding must be experimentally assessed. Such diagnostics are accomplished by applying high voltage to six electrodes, which are grounded in normal operation to form part of the Faraday shield. Our measurements place a constraint on the DC Stark shift at the 10^{-20} level, in units of the clock frequency. Moreover, we discuss a potential source of error in strategies to precisely measure or cancel non-zero DC Stark shifts, attributed to field gradients coupled with the finite spatial extent of the lattice-trapped atoms. With this consideration, we find that Faraday shielding, complemented with experimental validation, provides both a practically appealing and effective solution to the problem of DC Stark shifts in optical lattice clocks.

In the nearly seven decade-old quest to push the boundaries of atomic clock performance, and thus metrological capabilities in general, the elimination or precise evaluation of frequency shifts caused by external electromagnetic fields has been a persistent challenge [1, 2]. In modern-day optical lattice clocks, AC Stark shifts due to lattice light and blackbody radiation are two prominent examples [3, 4]. DC Stark shifts, attributed to nearby electronics or patch charges on the clock apparatus, have been observed as large as 10^{-13} [5] and pose a legitimate threat to state-of-the-art 10^{-18} clock performance (throughout, quoted shifts are understood to be in units of the clock frequency). Strategies to mitigate this threat include I) applying electric fields to measure and, if desired, cancel the stray-field shift [5–9], or II) enclosing the atoms by equipotential conductive surfaces, furnishing them with a field-free environment [10–13]. DC Stark shifts have also been estimated from apparatus geometry and material properties [14, 15]. Recently, Rydberg atoms were demonstrated as an *in situ* probe of the stray field in an optical lattice clock [16].

Here we identify a mechanism capable of compromising a Method I analysis, for which uncertainties at the 10^{-19} level have been reported. Using a simple model, we demonstrate how field gradients coupled with finite spatial extent of the lattice-trapped atoms can lead to appreciable clock error. Generally, the error scales with the measured stray-field shift. In principle, such error can be reduced by minimizing the stray field itself, which is precisely the objective of Method II. Unfortunately, practical constraints preclude surrounding the atoms with an ideal, continuous Faraday cage. Moreover, even conductive surfaces can acquire patch charges, a known concern for electrodes in ion clocks [17]. Consequently, a residual shift may remain, and quantifying an upper bound may be challenging. Seemingly, an optimal solution combines the attributes of Methods I and II. We demonstrate this combined approach in an ytterbium optical lattice clock, with measurements confirming the absence of a stray-field shift at the 10^{-20} level.

Given a uniform static electric field $\mathbf{E}$, the clock acquires a frequency shift $\delta\nu = kE^2$, where $E = |\mathbf{E}|$ and k is specific to the clock transition. Namely, $k \equiv -(\alpha_e - \alpha_g)/2h$, where h is Planck's constant and $\alpha_{g,e}$ are the static polarizabilities of the ground and excited clock states. To characterize blackbody radiation shifts, the coefficient k has been accurately measured for both Yb and Sr clock transitions [18, 19].

In practice, the lattice-trapped atoms have finite spatial extent, and the electric field may be nonuniform over this extent. Thus, a more complete representation of the clock shift is $\delta\nu = k \left\langle E^2 \right\rangle$, where $\langle \cdots \rangle$ denotes an average over the atoms. Generally, $\mathbf{E}$ is composed of both stray and applied fields. Given some nonzero stray field, it is evident that a true null shift can only be achieved if the applied field identically cancels the stray field across the entire atomic extent.

To illustrate the role field gradients can play in Method I, we introduce a simple model that affords an analytical solution. The model is illustrated in Fig. 1(a) and amounts to a cylindrically symmetric boundary value problem for the fields. The vacuum apparatus is taken to be a hollow metallic cylinder sealed with glass windows. The cylinder is electrically grounded, while the windows carry uniformly distributed static charges q_1 and q_2 across their respective internal surfaces. The external surfaces are spanned by electrodes, to which opposite voltages $+V$ and $-V$ are applied. With the electrodes grounded ($V = 0$), a stray field exists due to the charges. For $V \neq 0$, the electrodes further introduce an applied field. A one-dimensional optical lattice aligned with the symmetry axis confines the atoms with negligible radial extent and Gaussian axial distribution $(2\pi s^2)^{-1/2} \exp\left(-z^2/2s^2\right)$, with z being the distance from the center of the vacuum apparatus. The windows are separated by a distance ℓ and have diameter d, thickness t, and dielectric constant ϵ. Expressions for the electric potential within the vacuum region can be found in the
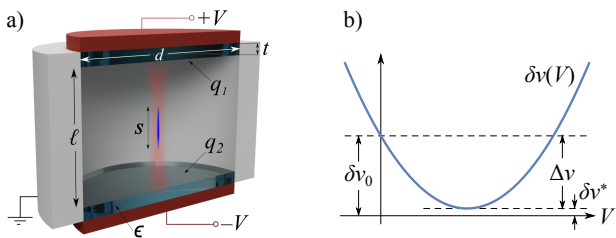
FIG. 1. a) Section view of the clock model described in the text. b) Corresponding clock shift $\delta\nu(V)$, with the quantities $\delta\nu_0$, $\delta\nu^*$, and $\Delta\nu$ introduced in the text. For $k > 0$ ($k < 0$), the extremum is a minimum (maximum) and all three quantities are positive (negative).

Supplemental Material (SM) [20].

As demonstrated on a more general basis below, the clock shift has the functional form

$$\delta\nu(V) = \delta\nu_0 + aV + bV^2. \tag{1}$$

The coefficients a and b are experimentally accessible parameters whose values may be determined by modulating V and observing the clock response. Specifying the clock shift for any V requires further knowledge of the stray-field shift $\delta\nu_0$. Towards this goal, we consider the extremum value of $\delta\nu(V)$, denoted $\delta\nu^*$. The stray-field shift $\delta\nu_0$, the extremum shift $\delta\nu^*$, and the difference between them $\Delta\nu \equiv \delta\nu_0 - \delta\nu^*$ are depicted in Fig. 1(b). In contrast to $\delta\nu_0$ and $\delta\nu^*$, $\Delta\nu$ is accessible through modulation of V. Invoking elementary calculus with Eq. (1), we find $\Delta\nu = a^2/4b$.

Let us initially neglect the atomic extent, taking the limit $s \to 0$. In this case, there exists a V for which the applied field identically cancels the stray field at the atoms, resulting in a null clock shift. This necessarily coincides with the extremum of $\delta\nu(V)$, as any other V yields a nonzero clock shift of definite sign (determined by k). This implies $\delta\nu^* = 0$, and it follows that $\delta\nu_0$ may be inferred from $\Delta\nu$ according to $\delta\nu_0 = \Delta\nu$.

The above reasoning breaks down for nonzero s, as we can no longer expect there to be a V such that the applied field identically cancels the stray field over the entire atomic extent. Consequently, $\delta\nu^*$ plays the role of a frequency correction for the field gradients. We write $\delta\nu^* = \eta\Delta\nu$, motivated by the fact that $\delta\nu^*$ and $\Delta\nu$ scale similarly with the stray field. Namely, a uniform scaling of the stray charge leaves η unchanged. The stray-field shift subsequently reads $\delta\nu_0 = (1 + \eta)\Delta\nu$. To leading order in s, we find $\eta = \zeta^2 s^2/\mathcal{R}^2$, where $\mathcal{R}$ is an effective length whose expression is given in the SM [20] and $\zeta \equiv (q_1+q_2)/(q_1-q_2)$ quantifies the charge-symmetry between the windows. Choosing $d = 150$ mm, $\ell = 100$ mm, $t = 10$ mm, and $\epsilon = 3.8$, $\mathcal{R}$ evaluates to $\mathcal{R} = 42$ mm. Further assuming $s = 1$ mm and 25% more charge on one window than the other, we obtain $\eta \approx 0.05$.

The example above suggests that the frequency correc-

tion $\delta\nu^*$ may be non-negligible if $\delta\nu_0$ itself is appreciable. More specifically, for an optical lattice clock exhibiting a stray-field shift above 10^{-18}, specification or cancellation of the shift at or below 10^{-18} may not be straightforward using Method I. There exists an additional burden in quantifying this correction or validating its neglect. Moreover, this effect could influence evaluations of other systematic effects. For example, lattice light shifts are typically characterized by varying lattice intensity, which may vary the atomic extent. Lastly, while our model suffices to demonstrate the potential importance of this effect, an actual system will inevitably be more complicated (lack symmetry in the apparatus, charge distribution, and atomic distribution; be an open-boundary system for the fields; contain dielectric surfaces in close proximity to the atoms; etc.). These complexities will presumably add to the difficulty of quantifying the correction due to field gradients.

From the preceding discussion, there is clear motivation for minimizing the stray-field shift. Recently, our group demonstrated an in-vacuum "shield" surrounding the lattice-trapped atoms in a Yb optical lattice clock [10]. An updated version is pictured in Fig. 2. The shield's objective is twofold: provide a well-defined, near-ideal room-temperature blackbody radiation environment and suppress stray electric fields. The shield body is a single copper structure, internally coated with electrically-conductive carbon nanotubes. BK7 windows for optical access have an electrically-conductive, ~ 5 nm-thick indium tin oxide (ITO) based coating. With the exception of two small apertures for atomic access, the copper body and ITO-coated windows collectively enclose the atoms. The design facilitates a Method I analysis. The windows are electrically isolated from the copper body using thin silicone spacers while being electrically connected to an external high-voltage source. We have independent control of the voltage on six windows, constituting three opposing pairs nominally aligned along mutually orthogonal axes. A seventh window is electrically connected to the copper body, which is permanently grounded.

The model introduced above, Fig. 1(a), is quasi-one-dimensional (we refer to it as the 1D model below). That is, although the stray and applied fields are derived from a three-dimensional boundary value problem, only the symmetry axis is sampled by the atoms, with the symmetry ensuring that the fields align (or anti-align) along this axis. Practical clocks, such as ours, demand a more general theory. To this end, we allow multiple voltage variables V_i. We assign to each electrode in the system a linear combination of the V_i, defining the voltage applied to that electrode. The total electric field is $\mathbf{E}_0 + \sum_i \mathbf{E}_i$, where $\mathbf{E}_0$ is the stray field (assumed independent of the V_i) and $\sum_i \mathbf{E}_i$ is the applied field with $\mathbf{E}_i \propto V_i$. The
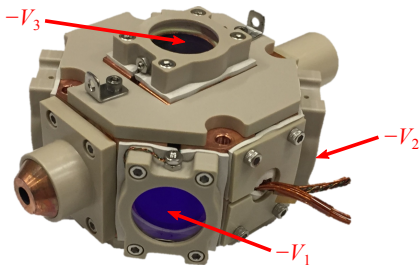
FIG. 2. Faraday shield described in the text, with ITO coated windows. Voltages $-V_1$, $-V_2$, and $-V_3$ are assigned to the indicated windows, with voltages $+V_1$, $+V_2$, and $+V_3$ assigned to the respective opposing windows (unlabeled). The shield body is a single copper structure, internally coated with carbon nanotubes. PEEK plastic secures the windows to the body, suppresses radiative heat exchange with the environment, and hides functional components including electrical wires, resistance temperature detectors, and film heaters. For loading the optical lattice, a thermal beam of atoms enters the shield through an aperture (pictured bottom left), while a counterpropagating beam of slowing light enters through an opposing aperture. Bundled electrical wires (pictured bottom right) proceed to vacuum feedthroughs. For scale, the windows are 1 inch in diameter.

clock shift subsequently reads

$$\delta\nu\left(V_1, V_2, \cdots\right) = \delta\nu_0 + \sum_i a_i V_i + \sum_{ij} b_{ij} V_i V_j, \qquad (2)$$

where $\delta\nu_0 = k\left\langle E_0^2\right\rangle$, $a_i V_i = 2k\left\langle \mathbf{E}_0 \cdot \mathbf{E}_i\right\rangle$, and $b_{ij} V_i V_j = k\left\langle \mathbf{E}_i \cdot \mathbf{E}_j\right\rangle$. Equation (2) is a generalization of equation (1) above. As before, we introduce the difference $\Delta\nu \equiv \delta\nu_0 - \delta\nu^*$, where $\delta\nu^*$ is the extremum with respect to all V_i. In terms of the coefficients in Eq. (2), $\Delta\nu$ reads [21]

$$\Delta\nu = \frac{1}{4} \sum_{ij} a_i a_j \left(b^{-1}\right)_{ij}, \qquad (3)$$

where the $\left(b^{-1}\right)_{ij}$ are related to the b_{ij} through matrix inversion (regarding the latter as elements of a matrix b and the former as elements of its inverse b^{-1}). We partition the problem of specifying $\delta\nu_0$ into two parts according to the sum $\delta\nu_0 = \Delta\nu + \delta\nu^*$. We initially focus on $\Delta\nu$, which represents the portion accessible through modulation of the V_i.

For our shield, we introduce a voltage variable for each opposing window pair, with voltages $-V_i$ and $+V_i$ assigned to the windows of each pair $i = 1, 2, 3$ (refer to Fig. 2). Given these assignments, the corresponding $\mathbf{E}_i$ are nominally uniform and mutually orthogonal at the atoms. In the limit this is strictly true, the b_{ij} with $i \neq j$ vanish and Eq. (3) reduces to

$$\Delta\nu = \sum_i \frac{a_i^2}{4 b_{ii}}, \qquad (4)$$

TABLE I. Induced frequency shifts relative to the fully-grounded arrangement, $\delta\nu\left(V_1, V_2, V_3\right) - \delta\nu_0$. Nonzero V_i are specified by sign only, with $|V_1| = |V_2| = 2$ kV and $|V_3| = 110$ V except where noted. Left and right data columns correspond to upper and lower signs in the voltage specifications and represent opposite polarity conditions.

(V_1 , V_2 , V_3)	induced shift $\left(\times 10^{-16}\right)$	
($\pm$, 0 , 0)	$-2.81(10)$	$-2.78(10)$
(0 , $\pm$, 0)	$-2.76(10)$	$-2.76(9)$
(0 , 0 , $\pm$)	$-2.77(7)^{\text{a}}$	$-2.67(7)^{\text{a}}$
(0 , 0 , $\pm$)[b]	$-915.2(4)$	$-915.6(4)$
($\pm$, $\pm$, 0)	$-6.21(9)$	$-6.09(9)$
($\pm$, $\mp$, 0)	$-5.15(9)$	$-5.09(10)$
($\pm$, 0 , $\pm$)	$-5.82(10)$	$-5.92(11)$
($\pm$, 0 , $\mp$)	$-5.60(10)$	$-5.55(11)$
(0 , $\pm$, $\pm$)	$-5.83(10)$	$-5.94(10)$
(0 , $\pm$, $\mp$)	$-5.49(10)$	$-5.41(10)$

[a] weighted mean of two measurement runs
[b] $|V_3| = 2$ kV

indicating that contributions to $\Delta\nu$ can be evaluated independently for each "direction" and summed up. However, nonorthogonality or nonuniformity of the $\mathbf{E}_i$ must be considered. This could be assessed through independent means, such as geometrical considerations and field modeling. A more reliable estimate exploits the atoms themselves. Either way, once assessed, these effects can be treated perturbatively, as highlighted in the SM [20].

Alternatively, without claiming *a priori* knowledge about the $\mathbf{E}_i$, here we use the general Eq. (3). We reserve Eq. (4) for future DC Stark shift assessments, where data from the present work can be leveraged to improve measurement efficiency and constrain deviations to this simple expression. We measure the induced shift $\delta\nu\left(V_1, V_2, V_3\right) - \delta\nu_0$ for various combinations of the arguments V_i. The V_i define a "test" configuration, with the fully-grounded configuration serving as a common reference. Each measurement run involves interleaving interrogations for the two configurations (test and reference) and recording the frequency difference. Table I presents our data. We ascribe to each measurement a statistical uncertainty commensurate with the Allan deviation at the end of the run, $\sim 1 \times 10^{-17}$. Voltage switching is enacted on the millisecond timescale, with spectroscopy initiated a few hundred milliseconds afterwards. Applied voltages are assessed with a voltage divider and found to be well-defined at the 2×10^{-4} fractional level. This introduces negligible uncertainty, with the exception of one line in Table I. For this data, large shifts were induced, -9×10^{-14}, with an uncertainty principally due to the applied voltage. All other induced shifts are at the 10^{-16} level. For each combination of V_i, measurements were performed under opposite polarity conditions.

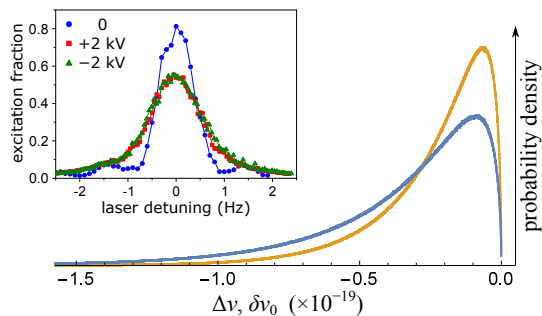A cursory examination of Table I reveals no statistically-significant difference under any polarity re-

FIG. 3. Main: Probability distributions for $\Delta\nu$ (yellow curve) and $\delta\nu_0$ (blue curve). The quantities are related by $\delta\nu_0 = (1 + \eta)\,\Delta\nu$; the $\delta\nu_0$ distribution is broadened relative to the $\Delta\nu$ distribution due to uncertainty from η (see text). Visible "noise" stems from the Monte Carlo evaluation. Inset: Excitation fraction versus laser detuning for the clock transition, without ($V_3 = 0$) and with ($V_3 = \pm 2$ kV) an applied field. $V_1 = V_2 = 0$ in each case. Detuning is referenced from the respective linecenter. A polarity-independent broadening accompanies the applied field.

versal. This invariance immediately suggests $\Delta\nu \approx 0$, though a more definitive analysis is clearly desired. Fitting Eq. (2) to the data in Table I allows determination of the coefficients a_i and b_{ij}, which can then be used to find $\Delta\nu$ via Eq. (3). We implement a Monte Carlo protocol [20] to map probability distributions for the data (interpreted as uncorrelated Gaussian distributions) into a probability distribution for $\Delta\nu$, the result of which is presented in Fig. 3. The distribution is clearly non-Gaussian and effectively constrains $\Delta\nu$ to negative values. The sign constraint is not surprising, considering all induced shifts are well-resolved negative (indicating $k < 0$ with near certainty, in agreement with the known value [18]). Based on this distribution, we assert a 68.3% confidence interval $-2.8 \times 10^{-20} < \Delta\nu < 0$ and a 95.5% confidence interval $-6.7 \times 10^{-20} < \Delta\nu < 0$.

In order to specify $\delta\nu_0$, we must further address $\delta\nu^*$. For any point near the shield's center, an arbitrary applied field can, in principle, be constructed with an appropriate choice of the V_i. It is therefore possible to cancel an arbitrary stray field at that point. However, it is generally not possible to cancel the stray field over some extended volume. In complete analogy to the 1D model, $\delta\nu^*$ plays the role of a correction for field gradients.

To explore the role of gradients in our clock, we consider the atomic spectra in the Fig. 3 inset, obtained with one-second-long Rabi excitation. The blue trace shows the spectrum when all electrodes are grounded (i.e., normal operation), yielding a ~ 1 Hz Fourier-limited linewidth. The red trace shows the spectrum with a large applied field ($V_1 = V_2 = 0$, $V_3 = +2$ kV). Because the lattice-trapped atoms are 1–2 mm from the symmetry plane between the charged windows, they experience a linear gradient from the applied field, resulting

in the observed inhomogeneous broadening (with broadening attributed to noise in the applied voltage smaller by an order of magnitude). The magnitude of this gradient is corroborated by finite element analysis [22]. Were a stray-field gradient also present, it could add to the applied-field gradient and the observed line broadening. Under opposite polarity conditions ($V_3 = -2$ kV), the applied field and its gradient reverse. In this case, the stray-field gradient would subtract from the applied-field gradient, reducing the observed line broadening. The green trace shows the observed spectrum upon polarity reversal. Since this reversal does not change the observed spectral linewidth and amplitude, a bound can be placed on the stray-field gradient. This technique benefits from the large applied field at the atoms, which amplifies broadening from a stray-field gradient. For this axis of measurement, the constraint is $|\delta\nu^*| < 2 \times 10^{-20}$.

While this technique could be repeated along the transverse lattice axes (where atomic extent is smaller and thus less sensitive to gradients) to constrain $\delta\nu^*$, here we exploit the fact that $\Delta\nu$ is essentially zero. As done previously for the 1D model, we write $\delta\nu^* = \eta\Delta\nu$, motivated by the fact that $\delta\nu^*$ and $\Delta\nu$ scale similarly with the stray field. While we lack a means to precisely evaluate η, the need is alleviated by our tight constraint on $\Delta\nu$. To investigate plausible values of η, we perform a finite element analysis of our shield plus atoms. Stray fields are introduced by applying patch voltages on internal shield surfaces (here η is unaffected by a uniform scaling of the patch voltages). Within the physical constraint $\eta \geq 0$, arbitrary values of η can be manufactured. Larger values require increasingly fine-tuned conditions. To realize $\eta > 1$, for instance, a high degree of symmetry is required between patch voltages on opposing sides of the shield; given a sufficiently symmetric arrangement, the atoms must then reside at a precise location. By examining various conditions, we take $\eta = 1$ as a conservative upper limit for our clock. A smaller value could be argued, but there is little incentive to be more aggressive or meticulous in light of our tight constraint on $\Delta\nu$.

Finally, we assume complete ignorance of η between zero and unity, assigning it a uniform probability distribution over this range. Combined with our results for $\Delta\nu$, we derive a probability distribution for $\delta\nu_0 = (1 + \eta)\,\Delta\nu$. Figure 3 presents the distribution, from which we assert a 68.3% confidence interval $-4.1 \times 10^{-20} < \delta\nu_0 < 0$ and a 95.5% confidence interval $-1.0 \times 10^{-19} < \delta\nu_0 < 0$. For comparison, the largest systematic uncertainties in our clock are presently at the 1×10^{-18} level [10, 23].

In conclusion, we have implemented Faraday shielding in an optical lattice clock and have constrained the stray-field DC Stark shift to below 10^{-19}. In contrast to optical lattice clocks that lack Faraday shielding and exhibit nonzero stray-field shifts, our normal operation does not require regular spectroscopic monitoring of the shift,

and there is no compromise to clock stability. Further measurements not part of this analysis, dispersed over multiple months and performed on independent Faraday-shielded clocks, have always yielded results consistent with zero stray-field shift. Here we have also identified a potential source of error in the measurement or cancellation of nonzero stray-field shifts attributed to field gradients. While exemplified for a Method I analysis, caution should generally be exercised. For example, the general approach put forth in Ref. [16], employing Rydberg atoms, could also be susceptible to error from field gradients; this may especially be the case if the spatial sampling provided by the ballistic Rydberg atoms differs from that of the lattice-trapped clock atoms. By combining the distinct attributes of Method I (applied fields) and Method II (Faraday shielding), we have demonstrated an effective means for tackling the problem of DC Stark shifts in optical lattice clocks.

This work was supported by NIST, NASA Fundamental Physics, and DARPA QuASAR. The authors thank W. Zhang and D. R. Leibrandt for their careful reading of the manuscript. This work is a contribution of the National Institute of Standards and Technology/Physical Measurement Laboratory, an agency of the U.S. government, and is not subject to U.S. copyright.

---

* kyle.beloy@nist.gov
† permanent address: State Key Laboratory of Advanced Optical Communication Systems and Networks, Institute of Quantum Electronics, School of Electronics Engineering and Computer Science, Peking University, Beijing 100871, China
‡ present address: Stable Laser Systems, Boulder, Colorado 80301, USA
§ permanent address: Department of Physics, Korea University, Seoul 02841, Republic of Korea
¶ permanent address: Niels Bohr Institute, University of Copenhagen, Blegdamsvej 17, 2100 Copenhagen, Denmark
** present address: Georgia Tech Research Institute, Atlanta, GA 30332, USA

[1] H. Lyons, Ann. New York Acad. Sciences **55**, 831 (1952).
[2] L. Essen and J. V. L. Parry, Nature **176**, 280 (1955).
[3] H. Katori, M. Takamoto, V. G. Pal'chikov, and V. D. Ovsiannikov, Phys. Rev. Lett. **91**, 173005 (2003).
[4] A. D. Ludlow, M. M. Boyd, J. Ye, E. Peik, and P. O. Schmidt, Rev. Mod. Phys. **87**, 637 (2015).
[5] J. Lodewyck, M. Zawada, L. Lorini, M. Gurov, and P. Lemonde, IEEE Trans. Ultrason. Ferroelectr. Freq. Control **59**, 411 (2012).
[6] S. Falke, N. Lemke, C. Grebing, B. Lipphardt, S. Weyers, V. Gerginov, N. Huntemann, C. Hagemann, A. Al-Masoudi, and S. Häfner, New J. Phys. **16**, 073023 (2014).
[7] B. J. Bloom, T. L. Nicholson, J. R. Williams, S. Campbell, M. Bishof, X. Zhang, W. Zhang, S. L. Bromley, and J. Ye, Nature **506**, 71 (2014).
[8] T. Nicholson, S. Campbell, R. Hutson, G. Marti, B. Bloom, R. McNally, W. Zhang, M. Barrett, M. Safronova, G. Strouse, W. Tew, and J. Ye, Nature Comm. **6**, 6896 (2015).
[9] M. A. Norcia, J. R. Cline, J. A. Muniz, J. M. Robinson, R. B. Hutson, A. Goban, G. E. Marti, J. Ye, and J. K. Thompson, arXiv:1711.10407 (2017).
[10] K. Beloy, N. Hinkley, N. B. Phillips, J. A. Sherman, M. Schioppo, J. Lehman, A. Feldman, L. M. Hanssen, C. W. Oates, and A. D. Ludlow, Phys. Rev. Lett. **113**, 260801 (2014).
[11] I. Ushijima, M. Takamoto, M. Das, T. Ohkubo, and H. Katori, Nat. Phot. **9**, 185 (2015).
[12] N. Nemitz, T. Ohkubo, M. Takamoto, I. Ushijima, M. Das, N. Ohmae, and H. Katori, Nat. Phot. **10**, 258 (2016).
[13] S. B. Koller, J. Grotti, S. Vogt, A. Al-Masoudi, S. Dörscher, S. Häfner, U. Sterr, and C. Lisdat, Phys. Rev. Lett. **118**, 073601 (2017).
[14] M. Pizzocaro, P. Thoumany, B. Rauf, F. Bregolin, G. Milani, C. Clivati, G. A. Costanzo, F. Levi, and D. Calonico, Metrologia **54**, 102 (2017).
[15] H. Kim, M.-S. Heo, W.-K. Lee, C. Y. Park, H.-G. Hong, S.-W. Hwang, and D.-H. Yu, Jap. J. Applied Phys. **56**, 050302 (2017).
[16] W. Bowden, R. Hobson, P. Huillery, P. Gill, M. P. A. Jones, and I. R. Hill, Phys. Rev. A **96**, 023419 (2017).
[17] D. J. Berkeland, J. D. Miller, J. C. Bergquist, W. M. Itano, and D. J. Wineland, J. Appl. Phys. **83**, 5025 (1998).
[18] J. A. Sherman, N. D. Lemke, N. Hinkley, M. Pizzocaro, R. W. Fox, A. D. Ludlow, and C. W. Oates, Phys. Rev. Lett. **108**, 153002 (2012).
[19] T. Middelmann, S. Falke, C. Lisdat, and U. Sterr, Phys. Rev. Lett. **109**, 263004 (2012).
[20] See Supplemental Material at (editor insert URL).
[21] If each combination of V_i does not provide a unique applied field *over the atomic extent*, then the matrix b is singular and lacks an inverse. In the limit of zero atomic extent, more than three voltage variables immediately implies a singular b.
[22] COMSOL Multiphysics® version 5.2a, www.comsol.com.
[23] R. C. Brown, N. B. Phillips, K. Beloy, W. F. McGrew, M. Schioppo, R. J. Fasano, G. Milani, X. Zhang, N. Hinkley, H. Leopardi, T. H. Yoon, D. Nicolodi, T. M. Fortier, and A. D. Ludlow, Phys. Rev. Lett. **119**, 253001 (2017).